International Journal of Pharmaceutics 423 (2012) 16–25

Contents lists available at ScienceDirect

International Journal of Pharmaceutics

journal homepage: www.elsevier.com/locate/ijpharm

A pharmaceutical study of doxorubicin-loaded PEGylated nanoparticles for magnetic drug targeting

J. Gautier[a,b], E. Munnier[a,b,*], A. Paillard[a,b], K. Hervé[a,b], L. Douziech-Eyrolles[a,b], M. Soucé[a,b], P. Dubois[a,b], I. Chourpa[a,b]

[a] Université François-Rabelais, EA 4244 «Physico-Chimie des Matériaux et des Biomolécules», équipe «Nanovecteurs Magnétiques pour la Chimiothérapie», Tours F-37200, France
[b] Institut Fédératif de Recherche 135 "Imagerie Fonctionnelle", Tours F-37000, France

ARTICLE INFO

Article history:
Received 17 February 2011
Received in revised form 25 May 2011
Accepted 6 June 2011
Available online 14 June 2011

Keywords:
Doxorubicin (DOX)
Superparamagnetic iron oxide nanoparticles (SPION)
Polyethylene glycol
Release kinetics
Intracellular distribution

ABSTRACT

One of the new strategies to improve cancer chemotherapy is based on new drug delivery systems, like the polyethylene glycol-coated superparamagnetic iron oxide nanoparticles (PEG-SPION, thereafter called PS). In this study, PS are loaded with doxorubicin (DOX) anticancer drug, using a pre-formed DOX–Fe^{2+} complex reversible at lower pH of tumour tissues and cancer cells. The DOX loaded PS (DLPS, 3% w/w DOX/iron oxide) present a hydrodynamic size around 60 nm and a zeta potential near zero at physiological pH, both parameters being favourable for increased colloidal stability in biological media and decreased elimination by the immune system. At physiological pH of 7.4, 60% of the loaded drug is gradually released from the DLPS in ~2 h. The intracellular release and distribution of DOX is followed by means of confocal spectral imaging (CSI) of the drug fluorescence. The in vitro cytotoxicity of the DLPS on MCF-7 breast cancer cells is equivalent to that of a DOX solution. The reversible association of DOX to the SPION surface and the role of polymer coating on the drug loading/release are discussed, both being critical for the design of novel stealth magnetic nanovectors for chemotherapy.

1. Introduction

Doxorubicin (DOX) is an antineoplastic agent of the anthracycline family frequently used in association with other drugs to treat a large number of cancers, like leukaemia, ovarian cancers and particularly last stage breast cancers (Lankelma et al., 1999). The clinical use of DOX is limited by its side effects, the most dangerous being a cumulative dose-dependent cardiotoxicity (Leonard et al., 2009). To minimize the side effects, DOX can be vectorized, that is associated to drug carriers that will favour its accumulation on the site of action and limit its dispersion in healthy tissues. Such a minimization has already been obtained with liposomal forms commercialized for nearly ten years (Leonard et al., 2009; Pütz et al., 2009). These forms increase the drug intratumoural concentration mainly due to their nanometric size: liposomes accumulate in tumours by a passive mechanism known as the enhanced permeation and retention effect (EPR effect). Indeed, the leaky fenestrations of neovasculature in tumours, combined with their inefficient lymphatic drainage, enable extravasation and accumulation of such small objects (Veiseh et al., 2010).

In addition to this passive targeting, nanovectors of a new generation are developed to permit an active targeting of tumours. Several concepts of active targeting are being investigated in the literature, namely at a molecular scale, as the functionalization of vector surfaces with targeting ligands complementary to specific or overexpressed receptors on cancer cells (Fan et al., 2010; Veiseh et al., 2010), or at a macroscopic scale, for example by means of an external magnetic field (Douziech-Eyrolles et al., 2007; Lübbe et al., 1996a,b, 2001; Maeng et al., 2010; Yang et al., 2010). Magnetic drug targeting is thus based on the association of a drug and magnetic nanoparticles. These magnetic drug delivery systems are essentially based on iron oxides (Aqil et al., 2008; Sabaté et al., 2008; Wassel et al., 2007; Ying et al., 2011), known to be non-toxic (Weissleder et al., 1989; Ying and Hwang, 2010).

To benefit from the EPR effect, the size of the final systems has to be below the dimensions of vascular permeativity in tumours, i.e. ~150 nm (Veiseh et al., 2010). The size of initial iron oxide nanoparticles is also determining for their magnetic properties:

* Corresponding author at: Laboratoire de Pharmacie Galénique, UFR de Pharmacie, 31 avenue Monge, 37200 Tours, France. Tel.: +33 247367201; fax: +33 247367198.
E-mail address: emilie.munnier@univ-tours.fr (E. Munnier).

0378-5173/$ – see front matter © 2011 Elsevier B.V. All rights reserved.
doi:10.1016/j.ijpharm.2011.06.010

below 30 nm diameter, the particles are superparamagnetic, i.e. highly magnetisable in the presence of magnetic fields but void of magnetic memory (remanence) (Mahmoudi et al., 2009). This is a critical requirement to avoid thrombotic risk related to magnetic aggregation of injectable delivery systems. The initial particles used for these purposes are commonly called SPION (superparamagnetic iron oxide nanoparticles) or USPIO (ultrasmall superparamagnetic iron oxide), the latter term being reserved for particle sizes below 20 nm (Roch et al., 2005).

The surface properties of the nanovectors are also essential for their biocompatibility. The presence of hydrophobic functions and/or charges favours nanoparticle opsonisation, i.e. nonspecific adsorption of plasma proteins (opsonins), which accelerates their recognition and elimination by the immune system before they reach their target tissue (Veiseh et al., 2010). In order to reduce the opsonisation and to ensure a colloidal stability by sterical repulsion, the surface of the magnetic systems must be coated with a hydrophilic and neutral moiety, such as a biocompatible polymer. For example, polymer molecules like polyethylene glycol (PEG) or dextran are known to reduce the opsonisation phenomenon and to lengthen the duration of circulation of the nanovectors (Harris and Chess, 2003). In addition, the coating can provide various chemical groups to conjugate drugs or targeting ligands (Wang and Thanou, 2010), in order to combine macroscopic and microscopic targeting. Nevertheless, the coating may lead to modified drug loading and release that must be taken into account (Zhu et al., 2010). The activity of the drug loaded on nanovectors must be respected through the formulation steps. The most common protocols of drug loading on the magnetic systems in the literature imply either covalent binding or entrapment of the drug into a polymer layer (Mahmoudi et al., 2010). Covalent linkage can be too strong to be cleaved by cellular enzymes, in particular if access to the drug is hindered by the polymeric coating (Shkilnyy et al., 2010). The entrapment of the drug within a polymer often leads to a burst effect (fast initial release) and/or to a low release in the absence of stimuli (Dilnawaz et al., 2010; Yang et al., 2010). We developed a novel method of reversible association of doxorubicin to SPION (Munnier et al., 2008): DOX is adsorbed on the iron oxide surface after being chelated with a Fe(II) ion (Fig. 1). The chelated iron binds to OH groups on the SPION surface and thus plays the role of an intermediary between the drug and nanoparticles. In this model, the drug release is pH-dependent as the DOX–Fe^{2+} complex dissociates in acidic conditions (Munnier et al., 2008). This release is expected to be tumour-specific, since the tumour environment is known to be more acidic than blood (Greulich et al., 2011; Medeiros et al., 2011). In addition, this method of reversible loading protects the drug activity: the DOX–Fe^{2+}–SPION systems were as active or even more so than a doxorubicin solution against MCF-7 human breast cancer cells in vitro (Munnier et al., 2008).

The aim of the present study is the loading of the doxorubicin–iron (II) pre-formed complex (DOX–Fe^{2+}, Munnier et al., 2008) on the PEGylated SPION developed by our group (Hervé et al., 2008). We propose a complete study of our model: the loading process is optimized, in order to maximize the quantity of doxorubicin bound, with a simple and easily transposable method. The optimized DOX-loaded PEGylated SPION are then characterized in terms of morphology, size and zeta potential. The in vitro doxorubicin release is investigated, in order to observe how PEGylation modifies the release. Biological aspects are also explored. Confocal spectral imaging is used to follow the subcellular distribution of doxorubicin after a treatment with the nanovectors and to determine the intracellular kinetics of action of the drug. Cytotoxicity assays permit to evaluate the anticancer activity of the nanovectors and to notice the effect of vectorization.

2. Materials and methods

2.1. Nanoparticle preparation

2.1.1. Materials

Doxorubicin hydrochloride was purchased from TEVA Pharmaceuticals Ltd. (Puteaux, France). Dulbecco's phosphate buffer saline (DPBS), ferric nitrate nonahydrate ($Fe(NO_3)_3{\cdot}9H_2O$), anhydrous ferric chloride ($FeCl_3$) and iron standard solution 1 g/L (titrisol) were purchased from Fisher Bioblock Scientific (Illkirch, France). Ferrous chloride ($FeCl_2$, $4H_2O$) was obtained from Acros Organics (Noisy Le Grand, France). 3-Aminopropyltrimethoxy silane (APTES), N-(3-dimethylaminopropyl)-N′-ethylcarbodiimide hydrochloride (EDC) and methoxypoly(ethylene glycol) 5000 propionic acid N-succinimidyl ester (activated PEG, aPEG) were purchased from Sigma Aldrich (Saint-Quentin-Fallavier, France). Sodium acetate and tris-(hydroxymethyl)-aminomethane (Tris) were provided by Merck (Fontenay-sous-Bois, France), and ferrous ammonium sulphate ($(NH_4)_2Fe(SO_4)_2{\cdot}6H_2O$) by Carlo Erba (Val de Reuil, France). In all the experiments, deionized water was used.

2.1.2. PEGylated SPION

The PEGylated ferrofluids were prepared according to a method described previously (Hervé et al., 2008). Briefly, superparamagnetic iron oxide nanoparticles (SPION) were synthesized by aqueous coprecipitation of ferric and ferrous chlorides in alkaline medium. In order to stabilize the surface chemical composition, SPION were oxidized by ferric nitrate and finally peptized in nitric acid and re-suspended in a determined volume of water. SPION were then silanized by a 12 h contact with APTES, washed and peptized in water at pH 3. Finally, SPION were PEGylated by a 24 h contact with aPEG, and purified by dialysis against water. These particles will be further mentioned as "PS" for PEGylated SPION.

2.1.3. Doxorubicin (DOX) loading on PEGylated SPION

PEGylated SPION (PS) were loaded with DOX via a DOX–Fe^{2+} complex, as described elsewhere (Munnier et al., 2008). DOX–Fe^{2+} complex was pre-formed by contact between DOX and a Fe^{2+} solution (1.5 M excess of Fe^{2+} over DOX) in Tris buffer pH 7.6. PS were incubated with DOX–Fe^{2+} complex in the dark, and harvested by centrifugation at 19,000 × *g* for 1 h at 4 °C. Several parameters were modified in order to optimize drug loading, as described in Section 3.1.

These particles will be further mentioned as "DLPS" for DOX-loaded PEGylated SPION.

2.2. Nanoparticle characterization

2.2.1. Morphology and size

The morphology of nanoparticles and their diameters were examined using a Philips CM20 electronic transmission microscope (TEM), operating at 200 kV. The samples were diluted in deionized water ($[Fe] \sim 10^{-3}$ g/L), then deposited on a carbon-coated copper TEM grid, the excess of solvent was removed with filter paper, and samples were left to air-dry before TEM viewing. The size estimation was based on 30 nanoparticles on 3 different images.

The hydrodynamic diameter of the particles was determined by DLS (Dynamic Light Scattering) technique with an Autosizer 2c (Malvern Instruments, Orsay, France) after sample dilution in deionized water ($[Fe] \sim 2 \times 10^{-3}$ g/L). Each measurement was performed at 25 °C, at least in triplicate, with a He–Ne laser (4 mW) operating at 633 nm, with the scatter angle fixed at 173°. The polydispersity index PDI is a measure of the broadness of a size distribution derived from the cumulative analysis of DLS data.

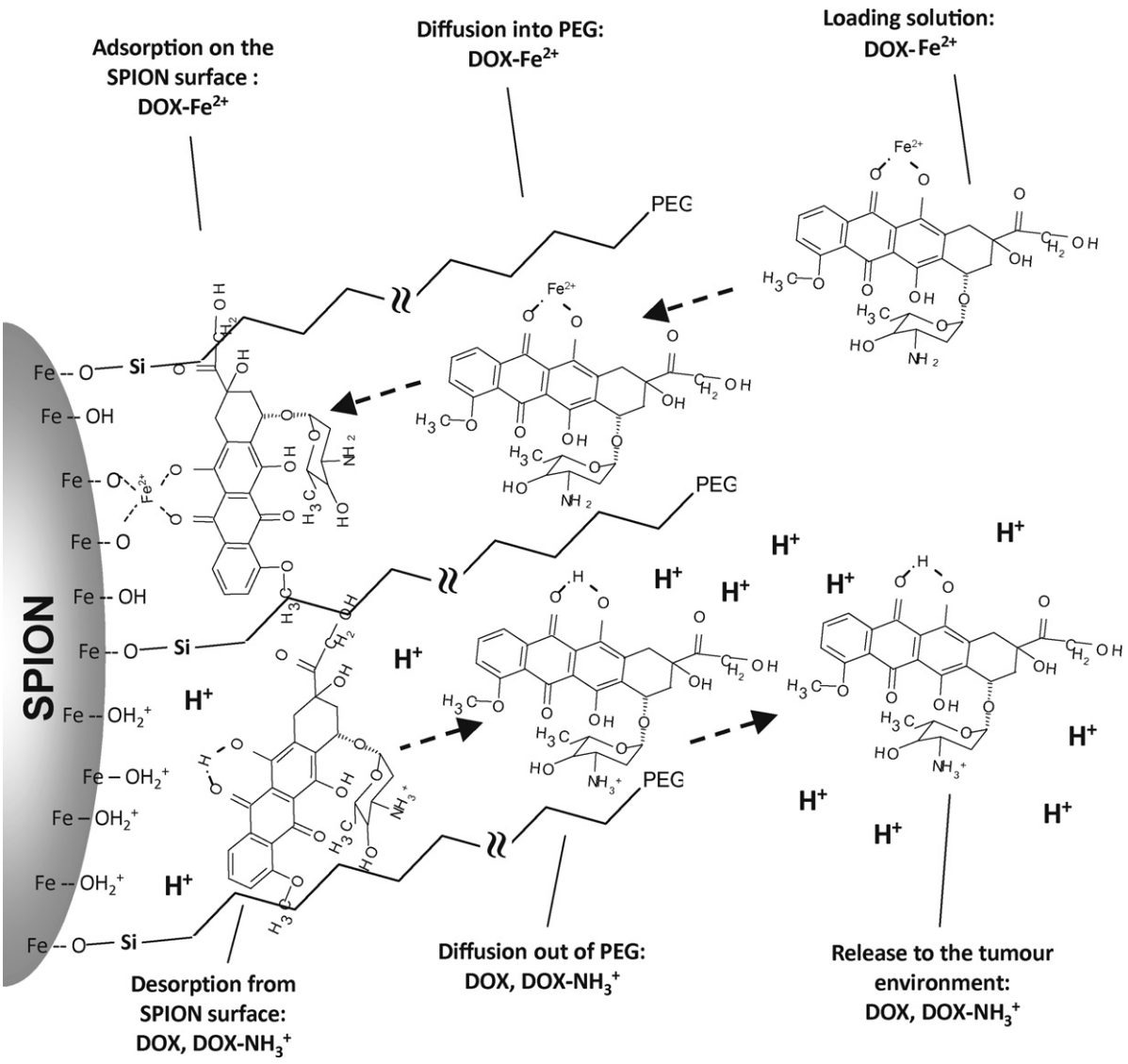

Fig. 1. Schematic diagram of loading of pre-formed DOX–Fe^{2+} complex and of release of DOX from the DLPS.

2.2.2. Zeta potential measurements

The zeta potential of the particles was determined using a Malvern NanoZ (Malvern Instruments, Orsay, France). Each measurement was performed at 25 °C, at least in triplicate, with a He–Ne laser (4 mW) operating at 633 nm, with a light scattering angle of 17°. Zeta potential was determined as a function of pH (ranging from 4.0 to 10.0) by means of a MPT-2 Titrator (Multi Purpose Titrator, Malvern Instruments, Malvern, UK) using HNO_3 and KOH 0.1 M.

2.2.3. Iron determination

The overall iron content in the ferrofluids is measured by atomic absorption spectrometry (iCE 3000 Series AA Spectrometer, ThermoFisher Scientific, France), after mineralization by a 12 h contact with HCl 6 N. A calibration curve was obtained with titrisol standard solution. Each determination was performed in triplicate. These results permit to estimate iron oxide concentration and mass in ferrofluid suspensions, considering that iron represents 71.5% w/w of SPION (Chourpa et al., 2005).

2.2.4. Drug loading determination

DLPS were suspended for 1 h in acetate buffer pH 4 in an ultrasonic bath to permit the total release of DOX, as the DOX–Fe^{2+} complex dissociates at low pH (Munnier et al., 2008). The sample was then centrifuged at 19,000 × *g* for 1 h at 15 °C. DOX concentration was determined in the supernatant by UV–visible spectrophotometry (Anthélie Advanced Spectrophotometer, Secomam, France), using its molar absorptivity determined at 500 nm. Each determination was performed at least in triplicate. Drug loading is expressed as the ratio of DOX mass over the mass of the iron oxide core of the nanovectors to permit a comparison with the non-PEGylated particles previously described (Munnier et al., 2008).

2.2.5. In vitro release kinetics of drug from DOX-loaded PEGylated SPION (DLPS)

Aliquots of DPLS suspensions, containing 10^{-4} g of iron, were made up to 2 mL with DPBS, continuously shaken and thermostated at 37 °C. At given time intervals, aliquots were centrifuged 1 h at 19,000 × *g* and 4 °C in order to separate the nanoparticles of the release medium. The drug concentration was determined in the supernatant from the intensity of the drug fluorescence at 557 nm (Hitachi F-4500 fluorescence spectrometer, excitation wavelength 500 nm), using a calibration curve.

2.3. Biological evaluation of DOX-loaded PEGylated SPION

For the biological evaluation, MCF-7 human breast carcinoma cells (American Type Culture Collection, LGC Promochem, Molsheim, France) were grown in Dulbecco's Modified Eagle Medium (DMEM) supplemented with 5% foetal bovine serum and 100 UI/mL penicillin G and 100 μg/mL streptomycin at 37 °C in a humidified 5% CO_2 atmosphere. All reagents were purchased from Fisher Bioblock Scientific (Illkirch, France).

2.3.1. Cytotoxicity evaluation of DOX-loaded PEGylated SPION

For cytotoxicity assays, cells were seeded for 48 h in standard 24-well plates (Cellstar, Greiner Bio-One, Courtaboeuf, France) at 1×10^4 cells per well. Then the culture medium was discarded and the cells were treated for 96 h with 500 μL of medium containing different doxorubicin concentrations (0.001–30 μM), either as DOX solutions or as DLPS suspensions (iron content from 1 μg/L to 333 mg/L). Cell viability was determined using a tetrazolium dye (MTT) assay (Mosmann, 1983). The cells were rinsed thrice with Hank's Buffered Salt Solution (HBSS) pH 7.4 and incubated for 4 h in 1 mL of medium containing 0.5 g/L of MTT. Then the medium was replaced by 500 μL of dimethylsulfoxide to dissolve the formazan crystals formed by viable cells. Absorbance was measured at 540 nm using a multiwell plate reader (ELX800, BioTek, Fisher Bioblock, Illkirch, France). The 50% inhibitory concentration (IC_{50}) was determined as the drug concentration that resulted in a 50% reduction in cell viability. All the experiments were performed in sextuplicate.

2.3.2. Confocal spectral imaging

Cover glasses of 1.4 cm^2 were coated with poly-D-lysine at 5 μg/mL in water for 1 h then placed in the wells of a 24-well plate. MCF-7 cells were plated (2×10^4 cells/well) and cultured for 24 h. The medium was then replaced by a suspension of DLPS in the culture medium at the concentration of 1 μM of doxorubicin. This incubation was made for 5, 30, 60, 120, 180 min at 37 °C/5% CO_2. After treatment, MCF-7 cells were washed twice in HBSS and the cover glasses were then mounted for confocal spectral imaging observation on live cells at 37 °C. Fluorescence measurements were carried out using an XploraINV confocal microspectrometer (Horiba Jobin Yvon, Villeneuve d'Ascq, France) equipped with an automated X–Y–Z scanning stage, a low dispersion grating (600 grooves/mm) and an air-cooled CCD detector. The DOX fluorescence was excited using a 532 nm line of an Ar^+ laser. The fluorescence spectra were excited and collected in confocal mode, through the 60× LWD objective. Live treated cells were placed in a closed microscopy chamber (Harvard Instruments) thermostated at 37 °C. For each cell analysis, an optical section (*x*–*y* plane) situated at half-thickness of the cell was scanned with a step of 0.7 μm that provided maps containing typically ~900 spectra (0.05 s per spectrum). Both acquisition and treatment of multispectral maps were performed with LabSpec software. Subcellular drug distribution maps were established via analysis of both the intensity and shape of DOX fluorescence spectra, as described previously (Munnier et al., 2011). Briefly, each experimental spectrum was fitted using the least-squares method to a sum of the three reference spectra of doxorubicin (see the Section 3). The fitting errors were below 5% (typically 2–4%). The cellular autofluorescence was completely neglected, because of the absence of any significant fluorescence of the untreated cells under the conditions used (laser power 5 μW on the sample, 0.05 s per spectrum). No sample photodegradation was observed. The average quantitative information (fitting scores) was extracted from each spectral map and represented as histograms.

Table 1
Physico-chemical properties of colloids PS and DPLS ($n \geq 3$).

	PEGylated SPION (PS)	DOX loaded PEGylated SPION (DLPS)
Hydrodynamic diameter (nm)	68.0 (±2.4)	62.3 (±2.5)
Polydispersity index (PDI)	0.174 (±0.018)	0.140 (±0.030)
Zeta potential (mV), pH 4–11	16 (±7.2) to −17 (±4.6)	21 (±6.3) to −21 (±3.4)
Isoelectric point (IEP)	pH 7.65 (±0.14)	pH 7.28 (±0.10)
Loading (% w/w DOX/iron oxides)	–	3.07% (±0.04)

3. Results and discussion

3.1. Optimization of DOX loading to PS

The initial SPION were prepared according to a method described previously to obtain a cationic aqueous sol (Hervé et al., 2008; Section 2.1). SPION obtained in this manner typically presented a size of 8 ± 2 nm in TEM (data not shown). The colloidal stability in acidic medium is provided by electrostatic repulsion of $FeOH_2^+$ groups on the surface of SPION and is dependent on pH value (see Fig. 2). However, for neutral particles around pH 7.4, a coating with PEG can provide stability due to steric hindrance.

In order to bind the PEG chains to SPION, the nanoparticles were treated with 3-aminopropyltrimethoxysilane (APTES). This reactant provides (i) methoxy silane groups that react with the hydroxyl groups at the surface of SPION and (ii) amino groups necessary to create an amide bond with the activated ester group of aPEG (Hervé et al., 2008). These PEGylated SPION (PS) present an excellent colloidal stability due to steric repulsion, their surface being nearly neutral over a wide range of pH as demonstrated by zeta potential measurements (Fig. 2 and Table 1).

The PS are loaded with a pre-formed DOX–Fe^{2+} complex (Fig. 1), prepared as described elsewhere (Munnier et al., 2008): doxorubicin is incubated with Fe^{2+} ions to form a chelate by replacing the hydrogen of the C11 phenolic group of DOX under strictly controlled concentration and pH conditions (pH 7.6, 1.5 iron/DOX molar ratio).

The DOX–Fe^{2+} complex solution is then incubated with PS in an aqueous buffer pH 7.6 at room temperature, since increasing temperature up to 50 °C during incubation shows no incidence on DOX loading (data not shown). In contrast, loading depends on the DOX/PS ratio (w/w ratios of DOX/PS iron varied from 0.05 to 1) and the time of incubation (30 min to 24 h). The most representative results are presented in Fig. 3.

Previously described assays on non-PEGylated, citrate stabilized SPION (Munnier et al., 2008) showed no significant loading of free DOX, because of a lack of affinity of the drug to the surface of SPION. In contrast, using DOX–Fe^{2+} chelates, the drug loading on the citrated SPION attained 14.6 ± 0.5% DOX/iron oxide w/w (Munnier et al., 2008). In the present study, free DOX loading on PS is significant (up to 1.82 ± 0.19% DOX/iron oxide w/w). It indicates that an appreciable amount of drug is diffused and captured in the PEG layer. Under similar conditions, the loading with DOX–Fe^{2+} complex is higher: up to 3% DOX/iron oxide w/w (Fig. 3). Since no additional interaction between DOX–Fe^{2+} chelate and PEG can be expected, this increase in DOX loading should indicate that the chelate adsorption on the iron oxide surface still takes place underneath the PEG layer (Fig. 1). Therefore, the drug is loaded on the PS by two mechanisms: capture in the PEG layer (Dilnawaz et al., 2010; Lübbe et al., 1996a; Yallapu et al., 2010) and iron-mediated adsorption on the SPION surface (Munnier et al., 2008).

Modulating DOX–Fe^{2+} complex/PS iron ratio has an influence on the DOX loading (Fig. 3A). Indeed, the loading is ~1% for a DOX–Fe^{2+} complex/PS iron ratio of 0.05, but increases to ~3% for a ratio of 0.1.

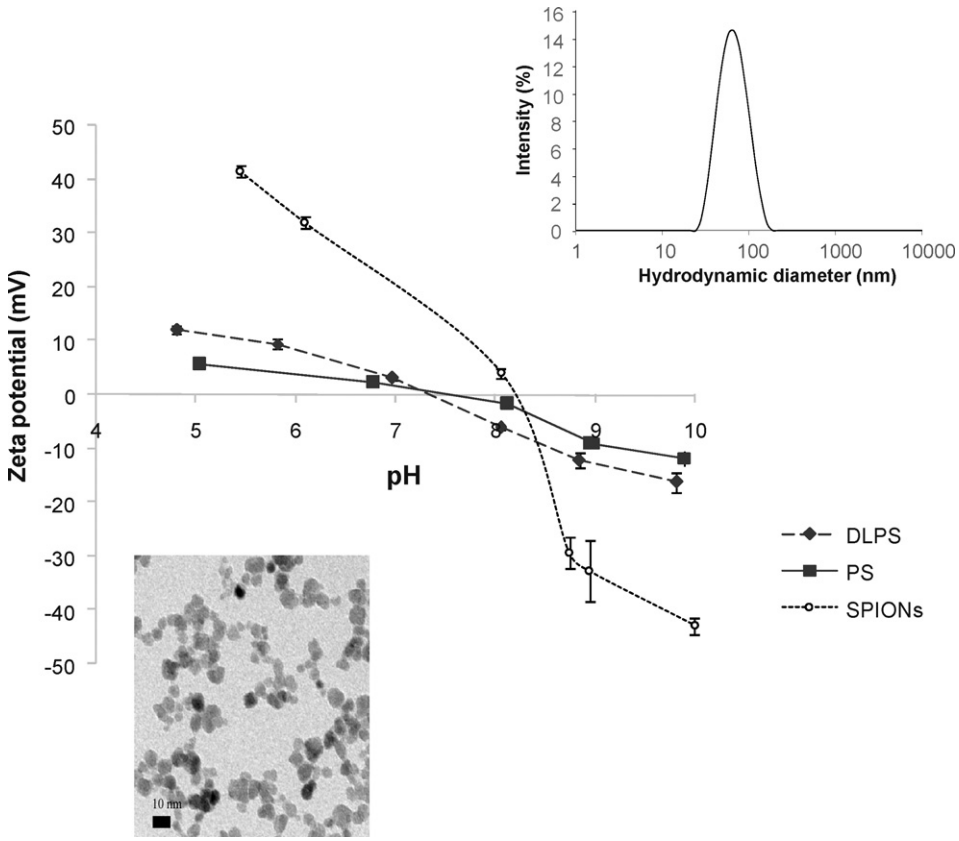

Fig. 2. Zeta potential versus pH for a batch (average of five determinations) of SPION and PEGylated SPION before (PS) and after DOX loading (DLPS). Insert: TEM image and hydrodynamic size distribution of DLPS ($n = 3$).

On the contrary, increasing the ratio to 0.5 and 1 does not seem to ameliorate the loading. The loading efficiency exhibits saturation: 27%, 7% and 3% of incubated drug was loaded respectively with ratios of 0.1, 0.5 and 1 DOX/PS iron (w/w).

The decreased DOX loading in DLPS (3%) compared to citrated SPION (14%, Munnier et al., 2008) is expected, since a part of the hydroxyl groups on the surface of SPION are occupied by silanes and/or silanes-PEG and the steric hindrance of PEG chains on the surface of SPION limits the access of the DOX–Fe^{2+} complex to the SPION surface.

In order to study the diffusion time necessary to cross the polymeric layer, we increased the incubation time from 15 min (data not shown) to 24 h. The drug loading increased between 15 and 30 min, stabilized for 2 h and decreased for 24 h (Fig. 3B). This decrease in drug loading may be due to a tendency of the complex in solution to dissociate or to precipitate over time, thus changing the equilibrium between free and PS-bound complex (Fiallo et al., 1999; Razzano et al., 1990). The results suggest that 30 min are enough to permit the DOX–Fe^{2+} complex to migrate through the PEG layer and that longer contact is useless to enhance loading, probably because of saturation of the PEG layers with the drug. The results described below correspond to DLPS prepared under the optimal conditions, i.e. 30 min incubation with DOX/PS iron ratio of 0.1 at room temperature. This method is sufficiently simple to be easily transposable for future therapeutic applications.

3.2. Physico-chemical characterization of DLPS

Transmission electron microscopy (TEM) permits to observe the morphology of the iron oxide nucleus and estimate its real

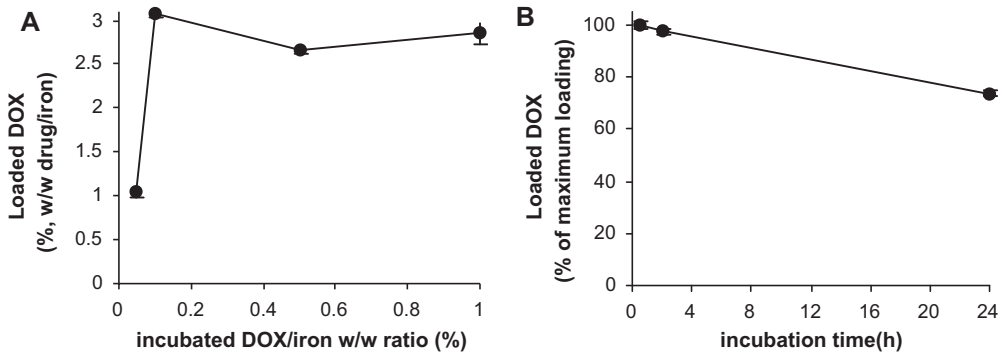

Fig. 3. DOX loading results under different conditions: (A) influence of incubated DOX/iron ratio for 30 min of incubation ($n = 3$); (B) influence of incubation time ($n = 3$) for DOX/iron ratio 0.5.

diameter. The DLPS appear to have a uniform roughly spherical shape (see insert in Fig. 2), with an average size of 10 nm ± 2 nm. These data are similar to those for SPION and PS obtained in our laboratory (Hervé et al., 2008; Munnier et al., 2008; Shkilnyy et al., 2010), and similar to those for other iron nanoparticles obtained by coprecipitation in the literature (Aqil et al., 2008; Rastogi et al., 2011; Yallapu et al., 2010). The TEM size of non-PEGylated and PEGylated particles is very similar because the polymer layer and the drug cannot be visualised on TEM images: these compounds have not sufficient electron density and their layers fold because of drying during sample preparation (Mahmoudi et al., 2010). The chemical composition of the organic layers, namely the presence of PEG and DOX, was confirmed respectively by means of FTIR and fluorescence spectroscopy (data not shown).

On the contrary, dynamic light scattering (DLS) permits to evaluate the hydrodynamic diameter of nanoparticles, which takes into account the drug/polymer layer. As shown in Table 1, values for DLPS are ~62 nm, which is close to those previously published for various PEGylated SPION (Hervé et al., 2008; Xie et al., 2007). The DLS measurements confirm the impression given by the TEM images: the distribution of the nanoparticles is monomodal (see insert in Fig. 2) with a satisfactory PDI smaller than 0.2 (see Table 1). This result shows that no large aggregates are present in the DLPS suspension.

The DLS results are completed by zeta potential measurements in function of the pH. For PS and DLPS, the zeta potential is close to zero over the pH range from 4 to 10 (Fig. 2). These results confirm prior observations (Hervé et al., 2008) and support the sterical nature of the colloidal stability of the suspensions. This implies that DPLS suspensions are physically stable in suspension at any pH, and particularly at physiological pH. We observe a slight decrease in hydrodynamic diameter (62 versus 68 nm, Table 1) and an increase in zeta potential for DLPS compared to PS. This slight modification of zeta potential cannot be due to a significant damage of the PEG layer, as the obtained profile is very far from the one of native SPION (see Fig. 2). One hypothesis could be that DOX ionizable functions, in particular the amino group ($pK_a \sim 8.2$) and the phenolic group at position C11 ($pK_a \sim 9.5$) influence the surface charge of DLPS. Nevertheless, taking into account the relatively low drug loading, and its major presence at the surface of SPION, the increased surface charge could not be directly induced by the presence of DOX in superficial PEG layers. The most plausible hypothesis seems to be that the decreased hydrodynamic diameter and the increased zeta potential are due to a change in spatial conformation of PEG chains in the presence of DOX.

Finally, the physical and chemical characteristics of DLPS like their small size, surface neutrality and good colloidal stability at physiological pH make them compatible with a systemic administration in vivo (Harris and Chess, 2003; Duan et al., 2008; Veiseh et al., 2010).

3.3. Kinetics of DOX release from DLPS

The in vitro release of DOX from DLPS was studied in a 24-fold donor/acceptor volume ratio to mimic the significant dilution of the suspension in the organism under physiological conditions of temperature and pH (37 ± 1 °C, DPBS buffer pH 7.4), as well as acidic pH to evaluate the pH dependence of the system (37 ± 1 °C acetic acid/sodium acetate buffer pH 4).

At pH 7.4, the kinetics observed with DLPS are progressive: no burst effect appears, DOX is released continuously during 2 h then reaches a plateau equivalent to ~70% of the loaded drug (see Fig. 4). The results demonstrate that the PEG layer does not prevent the drug to be released but delays this phenomenon at physiological pH.

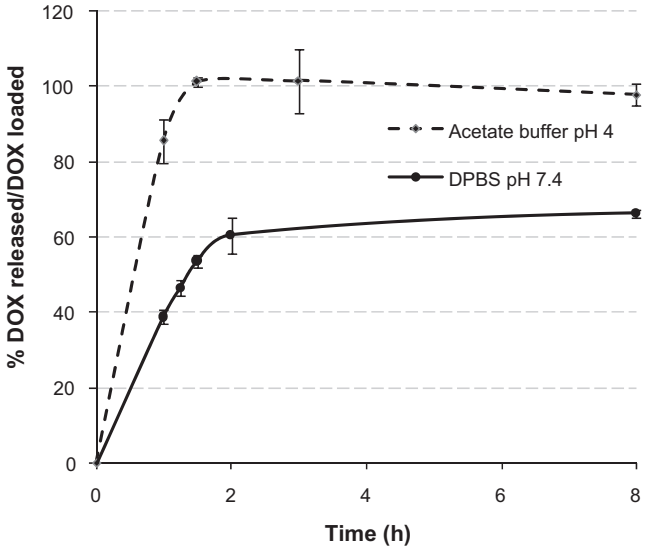

Fig. 4. In vitro release of doxorubicin from DLPS (DPBS pH 7.4, 37 °C, $n = 3$ and acetic acid/sodium acetate buffer pH 4, 37 °C, $n = 3$).

At pH 4, the release is considerably accelerated with 85% of the drug released in 1 h and practically total recovery within 2 h. A minimum duration of 1 h is imposed by the centrifugation step of the experiment, but our hypothesis is that the phenomenon is even faster, as the DOX–Fe^{2+} complex is not stable at pH 4 (Munnier et al., 2008). The time of release is then dependent on the time necessary to stabilization of the acidic pH near the SPION surface after diffusion through the PEG layer.

The kinetics at pH 7.4 seem adapted to magnetic drug targeting. In a clinical study, Lübbe et al. (2001) applied a magnetic field for 60–120 min in order to accumulate their vectors in the tumour. In our case, the moderate release during the first hour (~40% of loaded drug) should permit the nanoparticles to reach the therapeutic target without disseminating a high percentage of drug in the organism. This is important to limit the side effects generated by the free drug. In any case, this time seems reasonable compared to literature (2 weeks kinetics with glycerol monooleate coated magnetic nanoparticles loaded with paclitaxel and/or rapamycin for Dilnawaz et al., 2010; 200 h kinetics with wormlike polymer vesicles loaded with SPION and DOX for Yang et al., 2010). Once on the target, the more acidic pH of tumour tissue (Medeiros et al., 2011; Yan et al., 2007) should stimulate the release of the chelated DOX, but also of the entrapped DOX, which will then carry a positive charge on the sugar moiety (see Fig. 1). Naturally, we are conscious that the observed kinetics are only in vitro models and cannot be directly extrapolated to intracellular or in vivo kinetics. Under the experimental conditions, the appearance of a plateau indicates that a part of the loaded DOX is only slowly released from the DLPS. This kind of results is described in the literature for coated SPION. At pH 7.4, 33% of adsorbed DOX are released within 24 h from PEO-coated SPION (Maeng et al., 2010) and 31% in 48 h from composite polymer coated SPION (Rastogi et al., 2011). Our hypothesis is that the release of DOX is controlled by the drug diffusion through the polymer. In this case, the donor/acceptor volume ratio is decisive in the value of the plateau, and we can imagine that it would be displaced if the acceptor volume were larger. This is not the only explanation, since the ionic strength of the release medium may play a role in the rate of ion exchange at the surface of the SPION, as described in the literature (Li et al., 2008). Further studies could shed a light on how the DOX release from DLPS is modified in vivo. We will present some results of the intracellular release kinetics of the drug in the next section.

3.4. In vitro biological evaluation

3.4.1. Intracellular distribution and interaction of DOX delivered with DLPS

Intracellular doxorubicin release and subcellular doxorubicin redistribution are followed in living cells by confocal spectral imaging (CSI). In opposition to classical confocal fluorescence microscopy, the CSI collected not only the intensity of doxorubicin fluorescence at a given wavelength, but rather the total emission spectrum from each point scanned. This approach permits to distinguish very subtle modifications of doxorubicin intrinsic fluorescence (Fig. 5).

Three significantly different fluorescence spectra of intracellular DOX were detected in different cellular compartments (see reference spectra in Fig. 5A): a red-shifted spectrum in the nucleus and two more or less blue-shifted ones in cytoplasmic regions. Each intracellular spectrum of DOX was fitted as a weighted sum of these reference spectra. The fitting coefficients were used to generate specific maps (Fig. 5B) that can be merged and superimposed on a video image of the cell (Fig. 5D). In addition, the fitting coefficients can be statistically treated and presented in histograms (Fig. 5C).

As described before (Munnier et al., 2011), the nuclear spectrum (hereafter denoted nuc) is assigned to DOX intercalated into nuclear DNA. This corresponds only to DOX diffused through the cell membrane or intracellularly released from DLPS, since the nanoparticles cannot enter the nucleus. The two cytoplasmic spectra, denoted cyt1 and cyt2, correspond respectively to a lower and higher polarity of the molecular environment. These cytoplasmic spectra are very similar to those observed previously by Shkilnyy et al. (2010) for the cytoplasmic location of SPION–DOX–PEG where DOX was covalently bound to the SPION surface, i.e. deeply buried within the PEG layer. In the work reported by Shkilnyy et al., cells involved were MCF-7 cells as in our experiment, and the particles were similar, with a ~73 nm hydrodynamic size and were coated with PEG-5000. DOX remained fluorescent since it was bound through the amine group, outside of the fluorophore. In the present study, DOX bound to SPION by intermediate of Fe^{2+} is not fluorescent (Munnier et al., 2008). In contrast, iron-free DOX molecules entrapped/diffused inside the PEG layer are fluorescent and their fluorescence spectra are characteristic of their molecular environment within the PEG. As we determined previously, the PEG environment changes once the nanoparticles are inside cells (Shkilnyy et al., 2010). According to the blue-shifted spectral pattern of both cytoplasmic spectra, the PEG of intracellular particles creates a much more apolar environment for DOX, than when the particles are in aqueous buffer. Furthermore, this environment is even more apolar (more hydrophobic) than in the case when cells are incubated with DOX solution (Munnier et al., 2011). In general, such a blue shift of the emission spectrum is accompanied by an increase in fluorescent emission intensity. This kind of altering of the local environment around the fluorophore to a lower dielectric constant medium upon PEG–membrane interaction is known in the literature (Arnold et al., 1985). According to Ohki and Arnold (1990) PEG increases the hydrophobicity of contacting lipidic membranes by destabilizing their surface and by withdrawing free water from them. On the other hand, the decrease in dielectric constant of the PEG-related environment can be related to condensation of the PEG layers inside intracellular vesicles. This argument and the spectral similarity are both in agreement with internalization observed previously for DOX covalently bound to SPION covered with PEG (Shkilnyy et al., 2010).

From the logical consideration of the apolar environment and of the release kinetics, the major cytoplasmic fluorescence fraction (spectrum cyt1) should correspond to DOX molecules still entrapped in PEG (most apolar environment). The minor cytoplasmic fraction (spectrum cyt2) might be assigned to the drug molecules leaving the PEG layers and thus exposed to an increase of the polarity. As to a possible DOX fraction released from the particles outside the cells, under the conditions used, it is negligible in view of the recorded spectra (data not shown).

Thus, we are not able to exclude a small contribution of DOX of extracellular origin notably for nuclear fluorescence. Indeed, fluorescence of the doxorubicin administered as aqueous solution typically results in a strong nuclear staining (>90% of total intracellular drug) and a minor distribution in the cytoplasm (Munnier et al., 2011), which matches its main mechanism of action, inhibition of the nuclear enzyme DNA topoisomerase II (Hande, 2006). As it was determined before (Munnier et al., 2011) citrated SPION also deliver most of doxorubicin to the nucleus (more that 90% of fluorescence after 1 h incubation). However, when we used DLPS, the nuclear DOX fluorescence represents only 2.7% after 5 min and 22.8% after 3 h of incubation. In the latter case, the main fraction of the intracellular DOX is that of the spectrum cyt1 (Fig. 5). Thus, we deduce that the main cellular doxorubicin fluorescence did not come from doxorubicin released outside the cells, but from the drug carried by internalized nanoparticles.

The localisation of cyt1 fluorescence (Fig. 5) is concomitant with the internalization of PEGylated SPION by endocytose and accumulation inside intracellular vesicles like lysosomes as polymer nanoparticles (Harush-Frenkel et al., 2008). The kinetics of the intracellular drug distribution indicate slow migration of DOX from these cytoplasmic vesicles to the nucleus (cyt1 fluorescence is reduced from 97.5% after 5 min to 77.1% after 3 h, whereas nuc fluorescence increases from 2.7% to 22.8%). Interestingly, the cyt2 fluorescence increased temporarily during the first 30 min of incubation (2.2%) and then became negligible.

These data on subcellular DOX interaction and distribution confirm the interesting potential of PEGylated SPION as controlled delivery carriers for doxorubicin. The effect of this progressive release of doxorubicin on cellular viability is described in the next section.

3.4.2. Cytotoxicity

The aim of this biological evaluation was to determine if DOX loaded on DLPS still presents an antineoplastic activity. The CSI results described above showed that the entrance of DOX at its site of action, the nucleus, is delayed when it is vectorized by DLPS. According to these results, we chose to perform a cytotoxicity assay over 96 h in order to study the activity of the whole drug introduced in the medium. This duration corresponds to two cycles of division of MCF-7 cells, which guaranties the validity of the results. We compared the cytotoxicity on MCF-7 cancer cells of doxorubicin solution with DLPS with the same amount of loaded drug (Fig. 6). We demonstrated previously that neither drug-free SPION (Munnier et al., 2008) nor PEGylated SPION (Shkilnyy et al., 2010) adjusted for the same iron concentration produce any significant cytotoxicity on MCF-7 cells. For all concentrations tested in this study, both doxorubicin and DPLS have similar activity. The IC_{50} values are comparable for the two treatments and were determined to be 0.6 and 0.9 μM with doxorubicin and DLPS, respectively. These results show that our original loading process is reversible within 96 h and does not damage the DOX pharmacophore. The major mechanism of action of free doxorubicin is an intercalation in the DNA and an inhibition of the topoisomerase II (Hande, 2006). Several minor mechanisms of action are described in the literature as DOX-induced production of ROS (Minotti et al., 2004). As it is not very probable that the whole quantity of DLPS put into the well is internalized by the cell even in 96 h, the nanovectors could present a higher anticancer activity than the same amount of the free drug. We utter the hypothesis that in this case, several mechanisms of action are involved, as DOX has a different

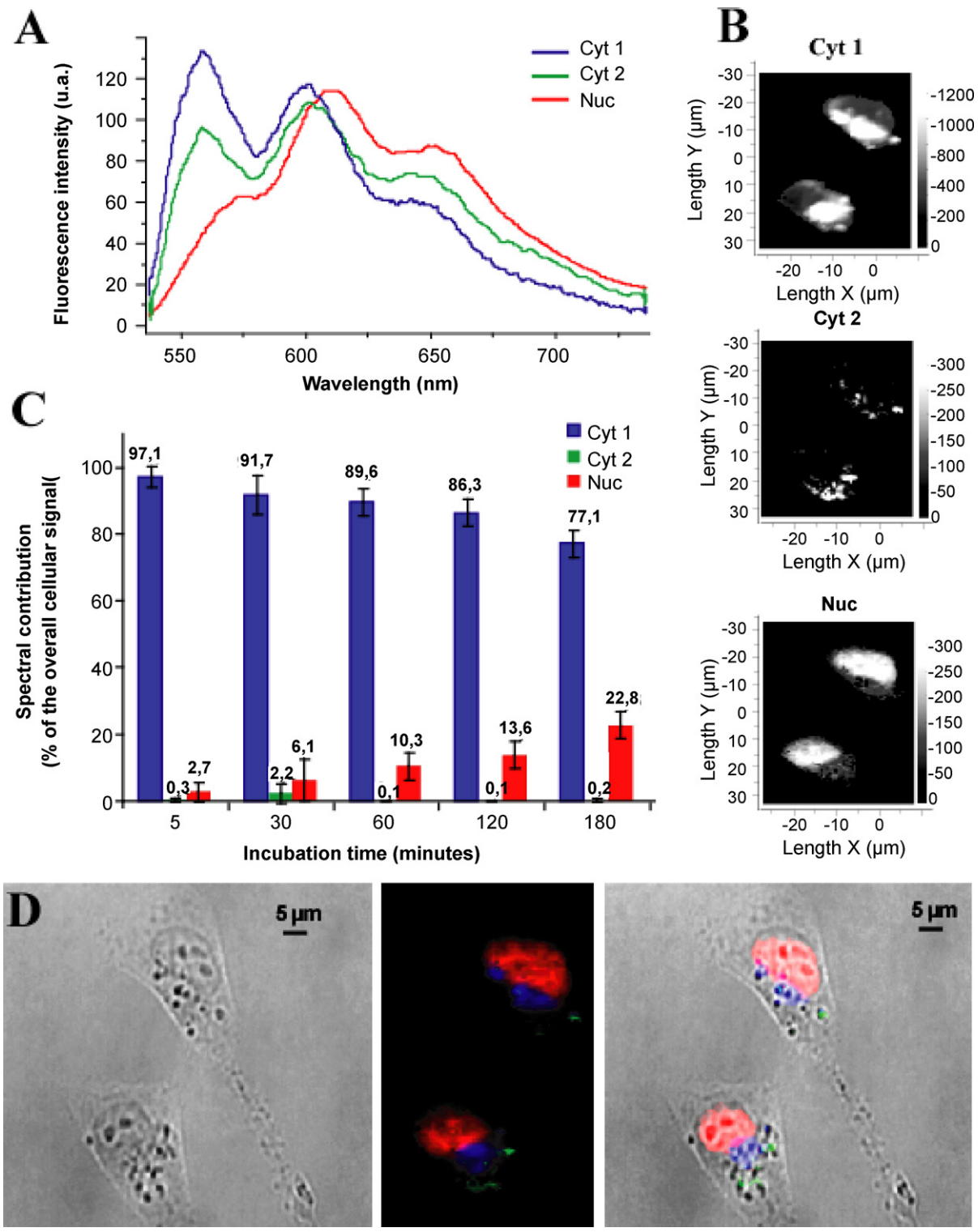

Fig. 5. Confocal spectral fluorescence imaging results on the subcellular DOX distribution in live MCF-7 cancer cells. (A) Reference spectra used to fit the intracellular DOX fluorescence: nuclear form (Nuc, red line) and two cytoplasmic forms (Cyt 1, blue line and Cyt 2, green line). (B) Typical subcellular distribution maps of the three reference spectra. (C) Statistically validated contribution to the cellular fluorescence of the three forms of fluorescence of DOX ($n \geq 6$). (D) Superposition of the maps using an extended intensity scale for colocalisation and encoded with pseudo colors. (For interpretation of the references to color in this figure legend, the reader is referred to the web version of the article.)

intracellular distribution from free DOX and DOX-loaded non PEGylated SPION (Munnier et al., 2011). The more plausible hypothesis is a joint action of DOX released in the culture medium within this long incubation time, which diffuses through the plasmic membrane, and of DOX released intracellularly. This hypothesis does not exclude the participation of supplementary mechanisms of action. Further studies can be useful to explore the mechanisms of action of these nanovectors, and to determine if they present a higher antineoplastic activity than the drug administered to cells as a solution.

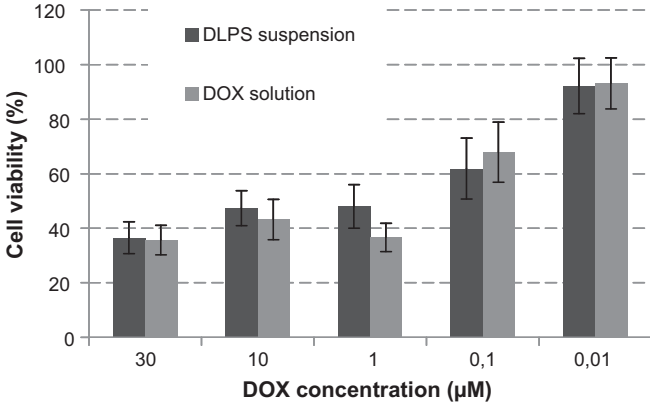

Fig. 6. Cytoxicity of DLPS versus DOX at equal drug concentration as measured on MCF-7 cancer cells (96 h, MTT assay).

4. Conclusion

The original approach of binding and pH-sensitive release of DOX to the SPION surface using a pre-formed DOX–Fe^{2+} complex is adapted to PEGylated SPION. This approach allows the preparation of DOX-loaded SPION carrying modest amounts of drug (~3% DOX/iron oxide, w/w). Nevertheless, the model is interesting in several respects. The drug is loaded on the particles following a simple and rapid protocol. The drug release kinetics is pH-dependent, and seems to be favourable for magnetic drug targeting. Moreover, drug cytotoxicity is preserved, and we suppose that several secondary mechanisms of action are involved. This study sheds a light on how PEGylation of the particles, often realized for the purpose of stealth, has an important influence on drug loading, drug release and nanoparticle distribution into the cell. Further studies will explore the cytotoxic potential of these DLPS in vivo.

Acknowledgments

This study was supported in part by grants from the Ligue Nationale contre le Cancer (Conseil Scientifique Inter-Régional Grand-Ouest (CSIRGO), Délégation Indre-et-Loire, France) and from the Region Centre, France (NANOMAG Project).

References

Aqil, A., Vasseur, S., Duguet, E., Passirani, C., Benoît, J.P., Roch, A., Müller, R., Jérôme, R., Jérôme, C., 2008. PEO coated magnetic nanoparticles for biomedical application. Eur. Polym. J. 44, 3191–3199.

Arnold, K., Herrmann, A., Pratsch, L., Gawrisch, K., 1985. The dielectric properties of aqueous solutions of poly(ethylene glycol) and their influence on membrane structure. BBA Biomembranes 815, 515–518.

Chourpa, I., Douziech-Eyrolles, L., Ngaboni-Okassa, L., Fouquenet, J.-F., Cohen-Jonathan, S., Soucé, M., Marchais, H., Dubois, P., 2005. Molecular composition of iron oxide nanoparticles, precursors for magnetic drug targeting, as characterized by confocal Raman microspectroscopy. Analyst 130, 1395–1403.

Dilnawaz, F., Singh, A., Mohanty, C., Sahoo, S.K., 2010. Dual drug loaded superparamagnetic iron oxide nanoparticles for targeted cancer therapy. Biomaterials 31, 3694–3706.

Douziech-Eyrolles, L., Marchais, H., Hervé, K., Munnier, E., Soucé, M., Linassier, C., Dubois, P., Chourpa, I., 2007. Nanovectors for anticancer agents based on superparamagnetic iron oxide nanoparticles. Int. J. Nanomed. 2, 541–550.

Duan, H.W., Kuang, M., Wang, X.X., Wang, Y.A., Mao, H., Nie, S.M., 2008. Reexamining the affects of particle size and surface chemistry on the magnetic properties of iron oxide nanocrystals: new insights into spin disorder and proton relaxivity. J. Phys. Chem. C 112, 8127–8131.

Fan, C., Gao, W., Chen, Z., Fan, H., Li, M., Deng, F., Chen, Z., 2010. Tumor selectivity of stealth multi-functionalized superparamagnetic iron nanoparticles. Int. J. Pharm., doi:10.1016/j.ijpharm.2010.10.038.

Fiallo, M.M.L., Garnier-Suillerot, A., Matzanke, B., Kozlowski, H., 1999. How Fe^{3+} binds anthracycline antitumour compounds. The myth and the reality of a chemical sphinx. J. Inorg. Biochem. 75, 105–115.

Greulich, C., Diendorf, J., Simon, T., Eggeler, G., Epple, M., Köller, M., 2011. Uptake and intracellular distribution of silver nanoparticles in human mesenchymal stem cells. Acta Biomater. 7, 347–354.

Hande, K.R., 2006. Topoisomerase II inhibitors. Update Cancer Ther. 1, 3–15.

Harris, J.M., Chess, R.B., 2003. Effect of pegylation on pharmaceuticals. Nat. Rev. Drug Discov. 2, 214–221.

Harush-Frenkel, O., Rozentur, E., Benita, S., Altschuler, Y., 2008. Surface charge of nanoparticles determines their endocytic and transcytotic pathway in polarized MDCK cells. Biomacromolecules 9, 435–443.

Hervé, K., Douziech-Eyrolles, L., Munnier, E., Cohen-Jonathan, S., Soucé, M., Marchais, H., Limelette, P., Warmont, F., Saboungi, M.L., Dubois, P., Chourpa, I., 2008. The development of stable aqueous suspensions of PEGylated SPION for biomedical applications. Nanotechnology 19, 465608, 7 pp.

Lankelma, J., Dekker, H., Luque, R.F., Luykx, S., Hoekman, K., van der Valk, P., van Diest, P.J., Pinedo, H.M., 1999. Doxorubicin gradients in human breast cancer. Clin. Cancer Res. 5, 1703–1707.

Leonard, R.C.F., Williams, S., Tulpule, A., Levine, A.M., Oliveros, S., 2009. Improving the therapeutic index of anthracycline chemotherapy: focus on liposomal doxorubicin (Myocet™). J. Breast 18, 218–224.

Li, Y., Wong, H.L., Shuhendler, A.J., Rauth, A.M., Wu, X.Y., 2008. Molecular interactions, internal structure and drug release kinetics of rationally developed polymer–lipid hybrid nanoparticles. J. Control. Release 128, 60–70.

Lübbe, A.S., Alexiou, C., Bergemann, C., 2001. Clinical applications of magnetic drug targeting. J. Surg. Res. 95, 200–206.

Lübbe, A.S., Bergemann, C., Huhnt, W., Fricke, T., Riess, H., Brock, J.W., Huhn, D., 1996a. Preclinical experiences with magnetic drug targeting: tolerance and efficacy. Cancer Res. 56, 4694–4701.

Lübbe, A.S., Bergemann, C., Riess, H., Schriever, F., Reichardt, P., Possinger, K., Matthias, M., Dörken, B., Herrmann, F., Gürtler, R., Hohenberger, P., Haas, N., Sohr, R., Sander, B., Lemke, A.J., Ohlendorf, D., Huhnt, W., Huhn, D., 1996b. Clinical experiences with magnetic drug targeting: a phase i study with 4′-epidoxorubicin in 14 patients with advanced solid tumors. Cancer Res. 56, 4686–4693.

Maeng, J.H., Lee, D.H., Jung, K.H., Bae, Y.H., Park, I.S., Jeong, S., Jeon, Y.S., Shim, C.K., Kim, W., Kim, J., Lee, J., Lee, Y.M., Kim, J.H., Kim, W.H., Hong, S.S., 2010. Multifunctional doxorubicin loaded superparamagnetic iron oxide nanoparticles for chemotherapy and magnetic resonance imaging in liver cancer. Biomaterials 31, 4995–5066.

Mahmoudi, M., Sant, S., Wang, B., Laurent, S., Sen, T., 2010. Superparamagnetic iron oxide nanoparticles (SPION): development, surface modification and applications in chemotherapy. Adv. Drug Deliv. Rev., 006, doi:10.1016/j.addr.2010.05.

Mahmoudi, M., Shokrgozar, M.A., Simchi, A., Imani, M., Milani, A.S., Stroeve, P., Vali, H., Hafeli, U.O., Bonakdar, S., 2009. Multiphysics flow modelling and in vitro toxicity of iron oxide nanoparticles coated with poly(vinyl alcohol). J. Phys. Chem. C 113, 2322–2331.

Medeiros, S.F., Santos, A.M., Fessi, H., Elaissari, A., 2011. Stimuli-responsive magnetic particles for biomedical applications. Int. J. Pharm. 403, 139–161.

Minotti, G., Menna, P., Salvatorelli, E., Cairo, G., Gianni, L., Anthracyclines:, 2004. molecular advances and pharmacologic developments in antitumor activity and cardiotoxicity. Pharmacol. Rev. 56, 185–229.

Mosmann, T., 1983. Rapid colorimetric assay for cellular growth and survival: application to proliferation and cytotoxicity assays. J. Immunol. Methods 65, 55–63.

Munnier, E., Cohen-Jonathan, S., Hervé, K., Linassier, C., Soucé, M., Dubois, P., Chourpa, I., 2011. Doxorubicin delivered to MCF-7 cancer cells by superparamagnetic iron oxide nanoparticles: effects on subcellular distribution and cytotoxicity. J. Nanopart. Res. 13, 959–971.

Munnier, E., Cohen-Jonathan, S., Linassier, C., Douziech-Eyrolles, L., Marchais, H., Soucé, M., Hervé, K., Dubois, P., Chourpa, I., 2008. Novel method of doxorubicin–SPION reversible association for magnetic drug targeting. Int. J. Pharm. 363, 170–176.

Ohki, S., Arnold, K., 1990. Surface dielectric constant, surface hydrophobicity and membrane fusion. Membr Biol. 114, 195–203.

Pütz, G., Schmah, O., Eckes, J., Hug, M.J., Winkler, K., 2009. Controlled application and scheduled removal of nanoparticle based chemotherapeutics (CARL) will reduce dose limiting adverse events in anticancer chemotherapy. Med. Hypotheses 72, 393–397.

Rastogi, R., Gulati, N., Kotnala, R.V., Sharma, U., Jayasundar, R., Koul, V., 2011. Evaluation of folate conjugated PEGylated thermosensitive magnetic nanocomposites for tumor imaging and therapy. Colloids Surf. B: Biointerfaces 82, 160–167.

Razzano, G., Rizzo, V., Vigevani, A., 1990. Determination of phenolic ionization constants of anthracyclines with modified substitution pattern of anthraquinone chromophore. Farmaco 45, 215–222.

Roch, A., Gossuin, Y., Muller, R.N., Gillis, P., 2005. Superparamagnetic colloid suspensions: water magnetic relaxation and clustering. J. Magn. Magn. Mater. 293, 532–539.

Sabaté, R., Barnadas-Rodríguez, R., Callejas-Fernández, J., Hidalgo-Álvarez, R., Estelrich, J., 2008. Preparation and characterization of extruded magnetoliposomes. Int. J. Pharm. 347, 156–162.

Shkilnyy, A., Munnier, E., Hervé, K., Soucé, M., Benoit, R., Cohen-Jonathan, S., Limelette, P., Saboungi, M.L., Dubois, P., Chourpa, I., 2010. Synthesis and evaluation of novel biocompatible super-paramagnetic iron oxide nanoparticles as magnetic anticancer drug carrier and fluorescence active label. J. Phys. Chem. C 114, 5850–5858.

Veiseh, O., Gunn, J.W., Zhang, M., 2010. Design and fabrication of magnetic nanoparticles for targeted drug delivery and imaging. Adv. Drug Deliv. Rev. 62, 284–304.
Wang, M., Thanou, M., 2010. Targeting nanoparticles to cancer. Pharmacol. Res. 62, 90–99.
Wassel, R.A., Grady, B., Kopke, R.D., Dormer, K.J., 2007. Dispersion of super paramagnetic iron oxide nanoparticles in poly(D,L-lactide-co-glycolide) microparticles. J. Colloids Surf. 292, 125–130.
Weissleder, R., Stark, D.D., Engelstad, B.L., Bacon, B.R., Compton, C.C., White, D.L., Jacobs, P., Lewis, J., 1989. Superparamagnetic iron oxide: pharmacokinetics and toxicity. Am. J. Roentgenol. 152, 167–173.
Xie, J., Xu, C., Kohler, N., Hou, Y., Sun, S., 2007. Controlled PEGylation of monodisperse Fe_3O_4 nanoparticles for reduced non-specific uptake by macrophage cells. Adv. Mater. 19, 3163–3166.
Yallapu, M.M., Othman, S.F., Curtis, E.T., Gupta, B.K., Jaggi, M., Chauhan, S.C., 2010. Multifunctional magnetic nanoparticles for magnetic resonance imaging and cancer therapy. Biomaterials, doi:10.1016/j.biomaterials.2010.11.028.
Yan, G.P., Robinson, L., Hogg, P., 2007. Magnetic resonance imaging contrast agents: overview and perspectives. J. Radiol. 13, e5–e19.
Yang, X., Grailer, J.J., Rowland, I.J., Javadi, A., Hurley, S.A., Steeber, D.A., Gong, S., 2010. Multifunctional SPIO/DOX-loaded wormlike polymer vesicles for cancer therapy and MR imaging. Biomaterials 31, 9065–9073.
Ying, E., Hwang, H.M., 2010. In vitro evaluation of the cytotoxicity of iron oxide nanoparticles with different coatings and different sizes in A3 human T lymphocytes. J. Sci. Total Env. 408, 4475–4481.
Ying, X.Y., Du, Y.Z., Hong, L.H., Yuan, H., Hu, F.Q., 2011. Magnetic lipid nanoparticles loading doxorubicin for intracellular delivery: preparation and characteristics. J. Magn. Magn. Mater. 323, 1088–1093.
Zhu, S., Hong, M., Tang, G., Qian, L., Lin, J., Jiang, Y., Pei, Y., 2010. Partly PEGylated polyamidoamine dendrimer for tumor-selective targeting of doxorubicin: the effects of PEGylation degree and drug conjugation style. Biomaterials 31, 1360–1371.